JOC The Journal of Organic Chemistry

Article

pubs.acs.org/joc

Comprehensive Experimental Study of N-Heterocyclic π-Stacking Interactions of Neutral and Cationic Pyridines

Ping Li, Chen Zhao, Mark D. Smith, and Ken D. Shimizu*

Department of Chemistry and Biochemistry, University of South Carolina, Columbia, South Carolina 29208, United States

Supporting Information

ABSTRACT: A comprehensive experimental study was carried out by measuring the relative strengths of parallel π-stacking interactions of N-heterocycles with nonheterocycles. A versatile and rigid model system was developed, which was in equilibrium between a "closed" conformation that forms an intramolecular π-stacking interaction and an "open" conformation that cannot form the interaction. First, the formation and geometries of the intramolecular N-heterocyclic π-stacking interactions were verified by X-ray crystallography. Next, the closed/open ratios were measured in solution via integration of the ^{1}H NMR spectra, providing an accurate comparison of the N-heterocyclic π-stacking interactions. The synthetic versatility of this model system enabled the systematic and comprehensive comparison of the influences of position, charge, and substituent effects of the nitrogen atom of the N-heterocycles within a single model system. The π-stacking interactions of the neutral N-heterocyclic rings were slightly stronger than that of nonheterocyclic rings. Cationic N-heterocycles formed significantly stronger π-stacking interactions than neutral N-heterocycles. The position of the nitrogen atom also had a strong influence on the stability of N-heterocyclic π-stacking complexes. Interestingly, opposite stability trends were observed for neutral and cationic N-heterocycles. For neural N-heterocycles, geometries with the nitrogen away from the π-face of the opposing ring were the more stable. For cationic N-heterocycles, geometries with the nitrogen close to the π-face of the opposing ring were the more stable. Finally, N-methylated heterocycles consistently formed stronger π-stacking interactions than N-protonated heterocycles.

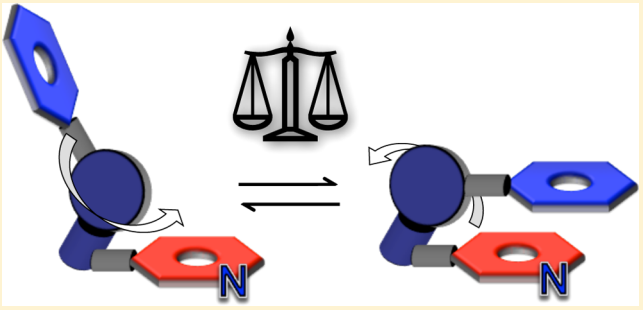

INTRODUCTION

Attractive noncovalent interactions between aromatic surfaces play an important role in many key molecular recognition processes.[1,2] The majority of π-stacking interaction studies, to date, have focused on the interactions of nonheterocycles, such as benzene,[3−7] and substituted benzene dimers.[8−19] Yet, N-heterocycles are ubiquitous in synthetic[20,21] and biological systems,[22] and their π-stacking interactions are often key to their function and utility.[23,24] The fewer experimental studies with N-heterocycles can be attributed to the greater synthetic challenge and the greater number of possible π-stacking geometries. Consequently, the majority of N-heterocyclic π-stacking studies have been theoretical computational studies.[25−30]

In this paper, we describe the development of a versatile and rigid molecular model system that can fix an N-heterocyclic and a nonheterocyclic ring into specific π-stacking geometries. The model system also provides a quantitative measure of the strengths of these interactions via their conformational equilibrium ratios (Figure 1). These "molecular balances" are in conformational equilibrium between "open" and "closed" conformations due to restricted rotation around a C_{aryl}−N_{imide} single bond. In the closed conformation, the rigid bicyclic framework forces the aromatic surfaces of the arm and shelf into an offset parallel π-stacking geometry. In the open conformation, these two surfaces are held apart. Therefore, the closed/open ratio provides a sensitive measure of the relative strengths of the intramolecular π-stacking interactions in solution.

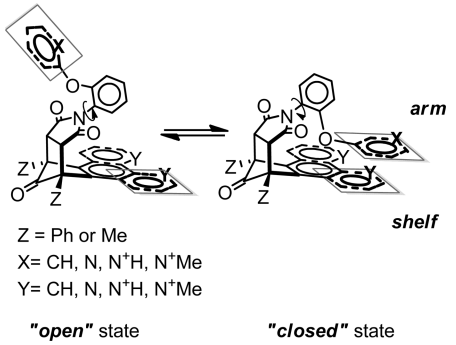

Figure 1. A general depiction of the molecular balance model system utilized in this study to measure the intramolecular N-heterocyclic π-stacking interactions formed in the closed conformer between an N-heterocyclic and a nonheterocyclic aromatic ring.

Received: March 4, 2013
Published: May 15, 2013

dx.doi.org/10.1021/jo400370e | J. Org. Chem. 2013, 78, 5303−5313

The structural rigidity and synthetic versatility of our molecular balance model system enabled the systematic study of the influences of the position, charge, and substituent of the nitrogen atom within a single molecular framework. This was important because of the much greater structural and geometric diversity of π-stacking complexes with N-heterocycles (Figure 2a) than with simple benzenes (Figure 2b). First, the nitrogen

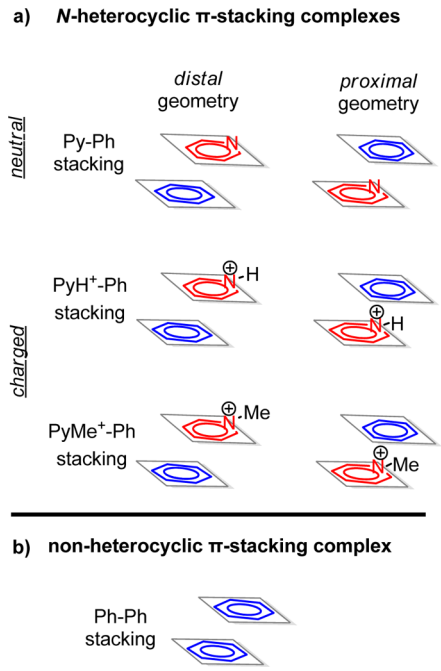

Figure 2. Comparison highlighting the greater structural and geometric diversity of the π-stacking complexes of (a) N-heterocycles versus (b) benzene rings.

atom disrupts the symmetry of the π-stacking complexes, giving rise to multiple geometries. These can be grouped into two distinct classes: the "distal" geometry, where the pyridine nitrogen is far from the π-face of the opposing benzene ring, and the "proximal" geometry, where the pyridine nitrogen is close to the π-face of the opposing benzene ring. Second, N-heterocyclic complexes can be neutral or charged via the absence or presence of a substituent on the nitrogen. Finally, the cationic N-heterocyclic complexes can have a proton or alkyl N-substituent.

Similar small molecule model systems that use conformational equilibriums to study noncovalent interactions have been widely employed with great success.[31] This includes the study of the π-stacking interactions of N-heterocycles. However, these studies have not been comprehensive and have primarily focused on specific pairwise comparisons. For example, Gellman and co-workers used a flexible secondary amide-based model system to demonstrate the enhanced affinity of a neutral six-membered heterocycle versus a phenyl ring.[32] Gung and co-workers also observed the stronger π-stacking interactions of an N-heterocyclic versus nonheterocyclic aromatic rings using a three-state triptycene-based model system.[33] Dougherty and co-workers used an electron-rich cyclophane aromatic host to measure the enhanced affinities of cationic versus neutral quinoline guests.[34] Waters and co-workers used a flexible rotamer model system to demonstrate that the position of the nitrogen atom in cationic π-stacking interactions had a profound influence on the interaction energies.[35] However, the results from these pioneering studies cannot be combined to quantitatively compare the stabilities of all of the N-heterocyclic π-stacking complexes shown in Figure 2.

To simplify these discussions, the following abbreviations will be used to describe the different complexes shown in Figure 2. The aromatic groups are abbreviated as follows: phenyl (Ph), pyridine (Py), pyridinium (PyH^+), *N*-methylpyridinium ($PyMe^+$). Thus, the interactions and complexes shown in Figure 2 (from top to bottom) are Py−Ph, PyH^+−Ph, $PyMe^+$−Ph, and Ph−Ph. In addition, we will use the term, "π-stacking", to describe the interactions shown in Figure 2 to maintain consistency with the literature. However, we realize this term is somewhat misleading because the $\pi-\pi$ interaction is repulsive.[36−39] The attractive components of π-stacking interactions are generally attributed to dispersion interactions of the molecular surfaces and electrostatic attraction between dipoles and/or quadrupoles of the aromatic rings.

RESULTS AND DISCUSSION

Molecular Balance Design. The molecular balance model system developed in this study has the same rigid bicyclic *N*-arylimide framework that we have successfully used to study face-to-face aromatic π-stacking (balance **1**)[40] and aliphatic CH−π[41] interactions (not shown). This similarity provided a number of advantages for the present study. First, the N-heterocyclic and nonheterocyclic aromatic surfaces could be predictably and precisely positioned relative to each other. We have previously demonstrated that the bicyclic framework fixes the arm and shelf aromatic surfaces into an offset parallel π-stacking geometry in the closed conformer.[40] The proximity of the two interacting surfaces in the closed conformers also prevents the formation of the other commonly observed edge-to-face, perpendicular geometry. Second, a series of molecular balances with N-heterocyclic units incorporated into either the arm or shelf surfaces can be rapidly assembled owing to the highly modular syntheses of this framework. Third, the closed/open ratios can be easily and accurately measured via the integration of the ^{1}H NMR spectra. The two conformers are in slow exchange at room temperature (23 °C), and differences as small as ±0.03 kcal/mol can be accurately measured. Fourth, the crystallinity of these molecular balances provided a unique opportunity to simultaneously characterize and study the geometry of N-heterocyclic π-stacking interactions in the solid state.

For this study, six new molecular balances (**2**−**7**) were developed (Figure 3). The intramolecular interactions in **2**−**7** mirror the different types of N-heterocyclic π-stacking complexes shown in Figure 2a. The relative position of the nitrogen atom in the complexes was controlled by placing the N-heterocyclic ring into either the arm or shelf. Incorporation of a pyridine ring into the aromatic arm of **2** yielded a molecular balance that adopts a distal geometry. The pyridine ring of the arm extends beyond the edge of the aromatic shelf so that the pyridine nitrogen is away from the π-face of the aromatic shelf. Conversely, incorporating pyridine rings into the arene shelf in **3** yielded a molecular balance that adopts a proximal geometry. In this case, the benzene arm extends out and over one of the nitrogens in the aromatic shelf. Similarly, cationic N-protonated and N-methylated balances with the N-heterocycles in the arm (**4** and **6**) adopt distal geometries and with the N-heterocycles in the shelf (**5** and **7**) adopt proximal geometries.

dx.doi.org/10.1021/jo400370e | J. Org. Chem. 2013, 78, 5303−5313

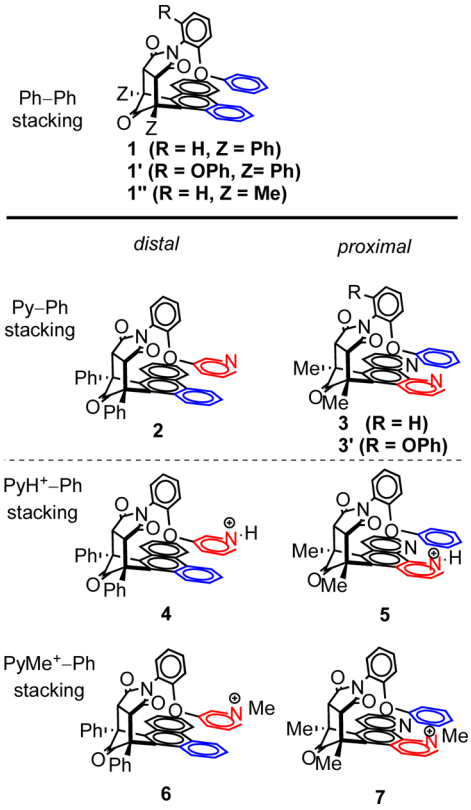

Figure 3. The closed conformers of molecular balances **1**–**7** that form intramolecular Ph–Ph, Py–Ph, PyH^+–Ph, and $PyMe^+$–Ph stacking interactions. The two interacting rings are highlighted in red (N-heterocycle) and blue (nonheterocycle). Balances **1′** and **3′** are two-armed analogues used in the crystallographic analysis, and balance **1″** is a control used to examine influence of the difference in bridgehead Z group over the closed/open ratios in solution.

Synthesis. The syntheses of balances with the N-heterocyclic ring in the arm (**2**, **4**, and **6**) followed the previously reported two-step convergent route.[40,41] A representative synthesis of **2** is shown in Scheme 1. First, the S_NAr reaction between 3-hydroxypyridine (**8**) and 2-fluoronitrobenzene (**9**) followed by Pd/C catalyzed reduction of the nitro group yielded aniline **10**.[42] The thermal condensation of aniline **10** with the endo-bicyclic anhydride **11** yielded the endo-bicyclic balance **2**. Pyridyl arms with the nitrogen in the meta position were prepared because the S_NAr reaction with the *para*-pyridyl precursor, 4-hydroxypyridine, was not successful due to preferential N- versus O-arylation.[43] Despite its lack of symmetry, the *meta*-pyridyl arm was able to adopt the desired distal geometry, as was later confirmed in the X-ray crystallographic and the solution ^1H NMR studies.

Incorporation of the N-heterocyclic rings into the shelf of balances (**3**, **5**, and **7**) required the synthesis of a new diene building block (**13**) that contained an N-heterocyclic phenanthroline shelf. Diene **13** was formed in two steps from the Knovenagel cyclization reaction of dione **12** and 2-pentanone followed by $SOCl_2$ dehydration of the mono-alcohol intermediate.[44] The Diels–Alder reaction between diene **13** and maleimide **14** gave the endo-bicyclic balance **3** (Scheme 2). The choice of 1,10-phenanthroline with two heterocyclic nitrogens as the shelf motif was intended to ensure the symmetry of the arene shelf, as the arene of arm can form π-stacking interactions with either of the two outer rings of the shelf.

In addition, two new control balances, **3′** and **1″**, were prepared. Balance **3′** is a "two-armed" analogue of **3**, which was synthesized from diene **11** and two-armed *N*-phenylmaleimide **15** (Figure 4) following the previously reported method.[40] Balance **1″** is a structural analogue of **1** with methyl groups instead of phenyl groups attached to the bridgeheads (Figure 1). Balance **1″** was prepared by a route similar to that for **3** via

Scheme 1. Syntheses of Balances 2 and 6[a]

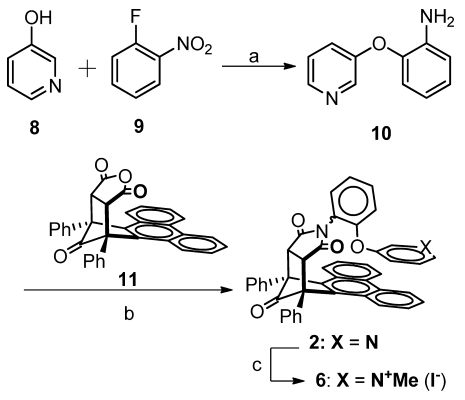

[a]Key: (a) i. Cs_2CO_3, 23 °C; ii. H_2, Pd/C, MeOH, 23 °C, 76% for two steps; (b) HOAc, reflux, 81%; (c) MeI, acetone, reflux, quantitative.

Scheme 2. Syntheses of Balances 3 and 7[a]

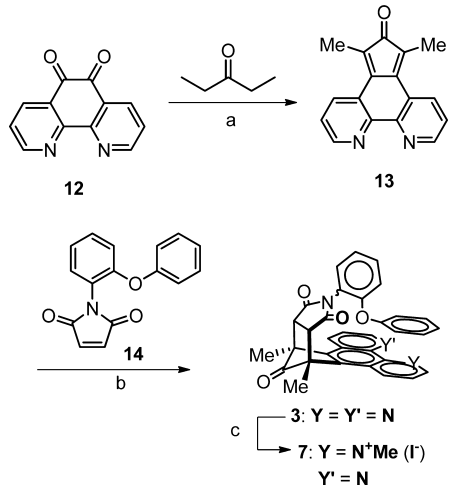

[a]Key: (a) i. K_2CO_3, MeOH, 23 °C; ii. py-$SOCl_2$, 23 °C, 37% for two steps; (b) CH_2Cl_2, pressure tube, 90 °C, 45%; (c) MeI, acetone, reflux, quantitative.

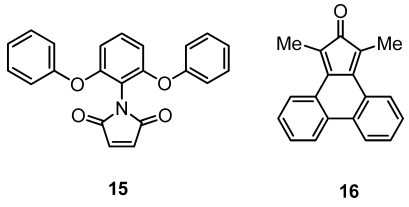

Figure 4. Maleimide **15** and diene **16** precursors used in the syntheses of the control balances **3′** and **1″**.

dx.doi.org/10.1021/jo400370e | J. Org. Chem. 2013, 78, 5303–5313

the Diels–Alder reaction between maleimide **14** and the known diene **16** (Figure 4).[45]

The cationic balances (**4**–**7**) were formed by methylation or protonation of the N-heterocycles in the arms or shelves. The N-methylated balances **6** and **7** were obtained through methylation of the neutral balances **2** and **3** using methyl iodide in acetone (Scheme 1 and 2). The protonated balances **4** and **5**, on the other hand, were obtained by in situ treatment of balances **2** and **3** with methanesulfonic acid.

X-ray Crystal Structure Analysis. To confirm the formation and correct geometry of the intramolecular N-heterocyclic π-stacking interactions in our model systems, the molecular balances were characterized using X-ray crystallography. X-ray quality single crystals of balances **2**, **3**, **4**, **6**, and **7** were successfully obtained from chloroform–acetonitrile mixtures; only balance **5** did not form X-ray quality crystals. All but one of the molecular balances crystallized in the closed conformation. This observation provided the first indication of the greater strength of the N-heterocyclic π-stacking interaction. In contrast, the nonheterocyclic π-stacking balance **1** consistently crystallized in the open conformation.[40] The only N-heterocyclic balance that crystallized in the open conformation was balance **3** that contains the weakest N-heterocyclic π-stacking interaction, as was later confirmed by the solution study. To characterize the intramolecular π-stacking interaction in balance **3**, a two-armed version **3′** was synthesized and crystallized. The presence of two identical phenyl ether arms attached to both ortho positions of the *N*-aryl rotor ensured that one arm would always adopt the closed conformation.

The crystal structures of **2**, **3′**, **4**, **6**, and **7** showed intramolecular parallel π-stacking interactions between the aromatic arm and shelf surfaces. Representative crystal structures of balances **2** and **3′** are shown in Figure 5. The rigid C-shaped endo-bicyclic framework brings the aromatic arm surface in close proximity to the aromatic shelf in the closed conformation. Examination of the geometries of the interacting six-membered rings confirmed the formation of the expected offset face-to-face π-stacking interactions in balances **2**, **3′**, **4**, **6**, and **7**. The center-to-plane distance distances (D) (Table 1) were 3.31–3.63 Å, which were well within the typical range of 3.3–3.8 Å for face-to-face aromatic stacking interactions.[46] The two rings were roughly parallel, as shown by the relatively small dihedral angles (α) (4.81°–17.04°) between the planes of the interacting rings, which were below the cutoff (<20°) for the face-to-face π-stacking geometry.[47] Finally, the centroid-to-centroid horizontal offset (H) of the two interacting rings (0.82–1.98 Å) compared favorably with the reported average value (1.30 Å) for the offset geometry in the literature.[46] (Definition for these geometric parameters is provided in Figure S2 in the Supporting Information)

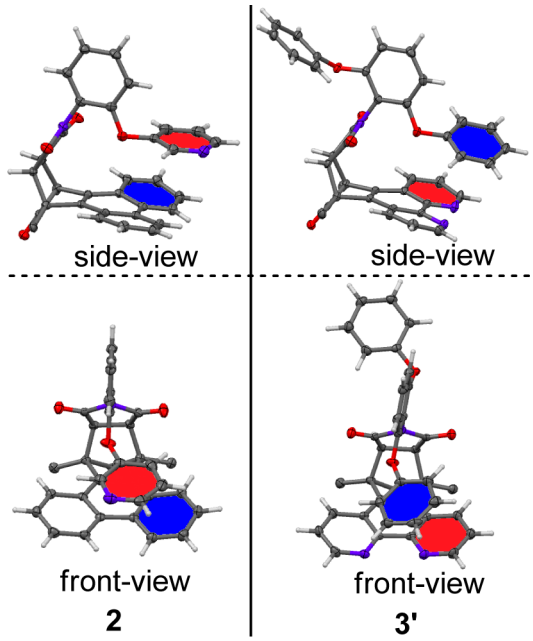

Figure 5. X-ray crystal structures of balances **2** and **3′** (the bridgehead phenyl and methyl functional groups are omitted for viewing clarity). The intramolecular N-heterocyclic π-stacking interactions are highlighted: N-heterocycle in red and nonheterocycle in blue.

Table 1. Measured Plane-to-Plane Angle (α), Centroid-to-Plane Distance (D) and Horizontal Centroid-to-Centroid Offset (H) between the Two π-Stacking Six-Membered Rings in the Crystal Structures of Balances 1′, 2, 3′, 4, 6, and 7

balance	π-stacking interaction	geometry	α	D [Å]	H [Å]
1′	Ph–Ph		7.8°[a]	3.75[a]	0.82[a]
2	Py–Ph	distal	9.3°	3.63	1.67
3′	Py–Ph	proximal	15.3°	3.60	1.82
4	PyH^+–Ph	distal	17.0°	3.37	1.27
6	$PyMe^+$–Ph	distal	4.8°, 6.4°[b]	3.29, 3.36[b]	1.78, 1.98[b]
7	$PyMe^+$–Ph	proximal	10.3°	3.31	1.65

[a]See ref 40. [b]The crystal structure of **6** contains two crystallographically independent molecules.

Analysis of the crystal structures also provided verification of the formation of the predicted proximal and distal π-stacking geometries. To better visualize the geometries, top views of the interacting rings in the crystal structures were compared (Figure 6). In particular, we were concerned that the mobility of the arene arm in the plane of the arene shelf might lead to alternative geometries. However, examination of each structure in Figure 7 shows the expected distal geometries in **2**, **4**, and **6** and the proximal geometries in the closed conformers of **3′** and **7**. We were also concerned with the ability of balances **3′**, **4**, and **6** to adopt the less favorable geometries (proximal, distal, and distal) for their respective N-heterocyclic π-stacking interactions. However, examination of these structures shows the N-heterocyclic nitrogen has been positioned in the designed geometry. This study confirmed the ability of the rigid framework to control the intramolecular interaction geometries.

Third, analysis of the crystal structures for balances **1′**, **2**, **3′**, **4**, **6**, and **7** confirmed the structural continuity of the intramolecular π-stacking interactions providing support for the ability to accurately compare their respective interaction energies. These new heterocyclic balances contained a much wider diversity of functional groups, charges, and geometries. We were concerned that they might lead to different secondary interactions and steric effects, which would mask the π-stacking interactions of interest. The similarity in the structures of the balances was demonstrated by the conformity of the positions of the ether oxygen linkers relative to their arene shelves. Figure

dx.doi.org/10.1021/jo400370e | J. Org. Chem. 2013, 78, 5303–5313

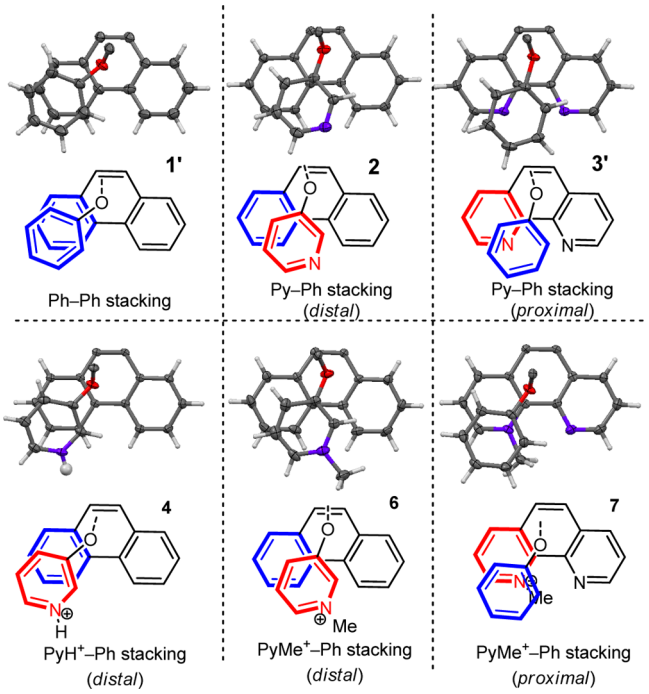

Figure 6. Top views of the crystal structures of balances **1′**, **2**, **3′**, **4**, **6**, and **7**, highlighting the intramolecular π-stacking interactions in the closed conformers. The corresponding ChemDraw representations are also provided for viewing clarity.

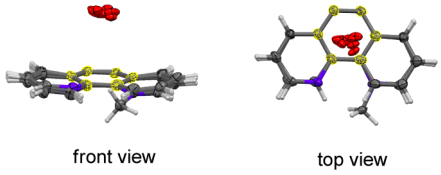

Figure 7. Top and front views of the overlaid crystal structures for balances **1′**, **2**, **3′**, **4**, **6**, and **7** highlighting the relative positions of the oxygen linkers on the arm over the arene shelves. Only the arene shelves and arm ether oxygens are shown, and the overlapping center six-membered aromatic ring of the shelves is highlighted in yellow.

7 shows the overlaid structures of the ether oxygen linkers and the arene shelves of the closed conformers **1′**, **2**, **3′**, **4**, **6**, and **7**. The position of the oxygen linkers was remarkably consistent among the seven crystal structures, confirming that the geometric and steric constraints in the closed conformers were very similar.

Characterization in Solution. The relative strengths of the intramolecular π-stacking interactions in the N-heterocyclic molecular balances were assessed by their closed/open equilibrium ratios. These were measured for balances **1**–**7** in solution via integration of their ^{1}H NMR spectra at 23 °C. The polar solvent DMSO-d_6 was chosen for these studies because of its ability to dissolve both the neutral and cationic balances. The equilibrium ratios were measured from the areas of the separate peaks for the open and closed succinimide methylene protons, which were singlets at ~4.9 ppm. The assignment of the open succinimide peak was made by matching its area to the distinct doublet of doublet for the open conformer's ortho proton of the *N*-aryl rotor, which was shifted drastically upfield (~4.5 ppm) because of its proximity over the aromatic shelf. The closed/open equilibrium ratios were converted to energies using the equation: $\Delta G = -RT \ln([\text{closed}]/[\text{open}])$. The closed/open ratio for balance **7** was estimated to be greater than 19:1 because only the closed conformer was observed.

For some of the cationic balances, the closed/open ratios were measured indirectly. The cationic N-protonated balances **4** and **5** were formed by adding MsOH to solutions of balances **2** and **3**, respectively. Unfortunately, in the presence of 1 equiv of MsOH, the broad water peak obscured the key succinimide singlets that were used to measure the closed/open ratios (see Supporting Information Figure S17). The closed/open ratios, however, could be accurately measured at lower equivalents (<1.0) of MsOH, and the equilibrium energies (ΔG's) were observed to change linearly with the amount of added MsOH (see Supporting Information Figures S17 and S18). Therefore, ΔG's for balances **4** and **5** were obtained from the linear extrapolation to 1 equiv of added MsOH.

Another concern was that the differences in the substituents at the bridgehead carbons of the balances might not allow accurate comparison. Balances **1**, **2**, **4**, and **6** have bridgehead phenyl rings, and balances **3**, **4**, and **7** had bridgehead methyl groups. Thus, balance **1″** with a bridgehead methyl group was prepared and compared with balance **1** with a bridgehead phenyl group. Balances **1** and **1″** had idential closed/open ratios in DMSO-d_6 (0.58 verus 0.53), suggesting that the bridgehead group did not influence the closed/open equilibrium ratio.

Quantitative Analysis of the Stability Trends. Comparison of the measured ΔG's for balances **1**–**7** is shown in Figure 8. Stronger π-stacking interactions in the closed conformer led

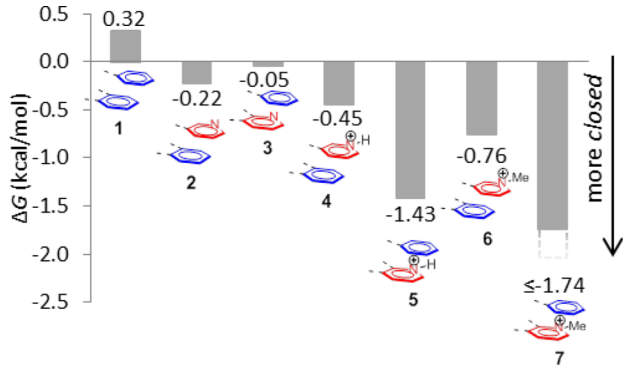

Figure 8. ^{1}H NMR measured ΔG's (kcal/mol) for balances **1**–**7** at 23 °C in DMSO-d_6 at 23 °C. The ChemDraw representation of the π-stacking interaction in each balance is shown. The uncertainty in ^{1}H NMR integration measurements gives an error of less than ±0.03 kcal/mol.

to higher closed/open ratios and more negative ΔG values. In general, the ΔG values were consistent with the expected N-heterocyclic π-stacking trends, confirming the ability of the balances to accurately compare these π-stacking interactions. For example, neutral N-heterocyclic balances **2**–**3** showed stronger π-stacking interactions than the nonheterocyclic balance **1**.[29] Cationic N-heterocyclic balances **4**–**7** also showed stronger π-stacking interactions than the neutral N-heterocyclic balances **2**–**3**.[27]

To facilitate the comparison of the respective π-stacking interactions, $\Delta\Delta G$'s were calculated for the N-heterocyclic balances **2**–**7** relative to the nonheterocyclic balance **1**, which contained the weakest π-stacking interaction (Table 2).

The neutral N-heterocyclic (Py–Ph) π-stacking interactions in balances **2** and **3** were found to be modestly stronger ($\Delta\Delta G$

dx.doi.org/10.1021/jo400370e | J. Org. Chem. 2013, 78, 5303–5313

Table 2. Measured Conformational Equilibrium Energies (ΔG, kcal/mol) for Balances 1-7 in DMSO-d_6 at 23 °C and Relative Energies (ΔΔG, kcal/mol) of the N-Heterocyclic Balances 2-7 Relative to the Nonheterocyclic Balance 1

balance	π-stacking interaction	geometry	ΔG^a	$\Delta\Delta G^b$
1	Ph−Ph		0.32	0.00
2	Py−Ph	distal	−0.22	−0.54
3		proximal	−0.05	−0.37
4	PyH^+−Ph	distal	−0.45	−0.77
5		proximal	−1.43	−1.75
6	$PyMe^+$−Ph	distal	−0.76	−1.08
7		proximal	≤−1.74[c]	≤−2.06

[a]DMSO-d_6, 23 °C; uncertainty less than ±0.03 kcal/mol. [b]$\Delta\Delta G = (\Delta G[\mathbf{x}] - \Delta G[\mathbf{1}])$; **x** = **2**−**7**; uncertainty < ±0.06 kcal/mol. [c]Only the closed conformer of balance **7** was observed on the ^{1}H NMR spectrum, and thus. $\Delta G[7]$ was estimated to be ≤−1.74 kcal/mol.

= −0.4 to −0.5 kcal/mol) than the nonheterocyclic (Ph−Ph) π-stacking interaction in balance **1**. This was consistent with the influence of the electronegative heterocyclic nitrogen that enhances the electrostatic attraction between rings as a result of the formation of a permanent dipole.[29] The magnitude of this trend compared favorably with the values measured by Gung and co-workers using their triptycene-based molecular model system.[33]

The cationic N-heterocyclic π-stacking interactions (PyH^+−Ph and $PyMe^+$−Ph) in balances **4**−**6** were found to be much stronger than the nonheterocyclic (Ph−Ph) π-stacking interaction in balance **1** (ΔΔG = −0.8 to ≤−2.1 kcal/mol) and also stronger than the neutral Py−Ph π-stacking interactions in balances **2**−**3** (ΔΔG = −0.2 to ≤−1.7 kcal/mol). This significant increase in strength was consistent with the greater electrostatic attraction arising from the cationic nitrogen ring and the π-cloud of the opposing aromatic surface.[27] This observation helps explain the prevalence of cationic N-heterocyclic π-stacking interactions in applications that rely on π-stacking interactions, such as biomimetic catalysis of S_N2 reactions,[48] conformational molecular switches,[49] diastereotopic control of stereoselective reactions,[50] and the threading of rotaxanes and catanenes.[51]

Influence of the Position of N-Heterocyclic Nitrogen. The rigidity of the bicyclic framework of this model system provided the unique opportunity to investigate how the relative position of the N-heterocyclic nitrogen atom influenced the stabilities of the π-stacking interaction; however, the ability of the molecular balances to maintain the distal and proximal geometries in solution was first verified. Balances **2**−**7** adopted the expected distal and proximal geometries in the solid-state; however, these geometries are more dynamic in solution. Computational studies of our model system have shown that the arene arm can sweep back and forth over the arene shelf.[52] Thus, the conformational equilibrium energies in solution of the proximal (**2**, **4**, and **6**) and distal (**3**, **5**, and **7**) balances were compared. Specifically, for each type of N-heterocyclic π-stacking interaction (Py−Ph, PyH^+−Ph, and $PyMe^+$−Ph), the energies of balances designed to adopt distal and proximal geometries were compared. In each case, the distal and proximal balances had distinctly different ΔG values. More importantly, the distal versus proximal stability trends for each type of interaction matched well the predictions of Hunter and Sander's electrostatic model.[53] This suggests that the balances were adopting the expected geometries in solution.

For the Py−Ph stacking interaction, the distal geometry (balance **2**) was found to be slightly stronger than the proximal geometry (balance **3**) by ΔΔG = −0.17 kcal/mol. Figure 9

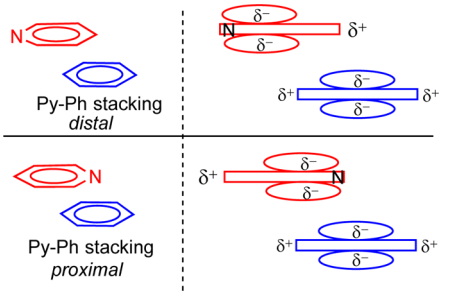

Figure 9. Schematic representations comparing the neutral Py−Ph π-stacking interactions in the proximal and distal geometries using Hunter and Sander's electrostatic quadruple model.

shows the electrostatic origins of this geometric preference. The electronegative nitrogen of the pyridine ring bears a partial negative charge (δ^-) and creates a partial positive charge (δ^+) on the opposite end of the ring. Thus, the distal geometry provides better electrostatic complementarity to the quadrupole of the opposing phenyl ring. The proximal geometry, on the other hand, lacks an electropositive hydrogen on the pyridine nitrogen which eliminates one of the attractive electrostatic interactions. In addition, the proximal geometry contains an additional repulsive interaction between the electronegative pyridine nitrogen and the π-surface of the opposing phenyl ring. The weaker proximal Py−Ph stacking interaction in balance **3** was also evident in the solid-state studies because balance **3** was the only balance that did not crystallize in the closed conformation.

For the cationic N-heterocyclic (PyH^+−Ph and $PyMe^+$−Ph) π-stacking interactions, the opposite geometric preference was observed. The proximal geometry (balances **5** and **7**) was considerably more stable than the distal geometry (balances **4** and **6**) by the same amount (≤−0.98 kcal/mol. The preference for the proximal geometry in the cationic N-heterocyclic π-stacking interactions can also be explained using Hunter's electrostatic model. The positive charge caused by protonation or alkylation of the pyridine is electrostatically attracted to the π-cloud of the opposing phenyl ring. This attractive force is stronger in the proximal geometry because the positively charged nitrogen is closer to the face of the opposing phenyl ring. The observed preference for the proximal geometry in PyH^+−Ph stacking interactions is also consistent with the "orientation effect" of the cationic π-stacking interactions observed by Waters and co-workers in their flexible folding model system.[35] Furthermore, the larger difference in energy between the proximal and distal geometries for the cationic ($|\Delta\Delta G| \geq 0.98$ kcal/mol) versus neutral ($|\Delta\Delta G| = 0.17$ kcal/mol) π-stacking interactions reinforced the electrostatic origins of these geometrical preferences.

Influence of the N-Substituent. Next, the influence of different N-substituents (methyl versus proton) in the cationic balances was analyzed. To isolate this variable from the geometric preference noted above, the proximal (**5** and **7**) and distal (**4** and **6**) balances were compared separately. For the proximal balances, the N-methylated balance **7** had a stronger π-stacking interaction than the N-protonated balance **5** by ΔΔG ≤ −0.31 kcal/mol. The greater stability of the proximal

dx.doi.org/10.1021/jo400370e | J. Org. Chem. 2013, 78, 5303−5313

N-methylated heterocycle complex was attributed to the ability of the *N*-methyl group to form an additional stabilizing CH−π interaction. Evidence for the additional CH−π interaction was provided by the crystal structure of balance **7**. As shown in Figure 10, a proton of the *N*-methyl group points toward the

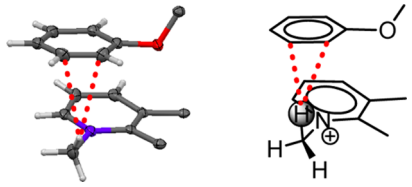

Figure 10. Truncated side view (left) of the crystal structure of closed-**7** highlighting the presence of a CH−π interaction between the proximal N-methylated heterocycle on the shelf and the phenyl ring on the arm. A ChemDraw representation is also provided (right). The short distance contacts between the *N*-methyl proton and phenyl carbon are highlighted with red dotted lines.

opposing phenyl ring with two short H−C distances (atom-to-atom distance) of 3.02 and 3.03 Å, respectively, which falls within the common cutoff distance (3.05 Å) for a CH−π interaction.[54] We have also observed that similar intramolecular CH−π interactions can stabilize the closed conformer of our *N*-arylimide bicyclic balances by up to −1.0 kcal/mol in organic solvents.[41] The supporting role of CH−π interactions in enhancing cation−π interactions of alkylated ammonium has been mentioned in several studies, such as the folding of a β-hairpin peptide and the in vitro binding of trimethyllysine to the HP1 chromodomain.[55]

A similar analysis was performed on the distal cationic balances (**4** and **6**); however, the equilibrium ratios of these distal balances were much more susceptible to solvent effects, which made the *N*-methyl versus N-proton preference solvent-dependent. These solvent effects are discussed in the next section.

Solvent Effects. The ability to measure the closed/open ratios in different solvents provided an additional method of probing the origins of the stability trends. Thus, the above analyses were also carried out in two additional organic solvents: $CDCl_3$ and CD_3CN. The measured relative energies are shown in Table 3. Overall, the similar stability trends were observed in all three solvents, providing further confirmation of the N-heterocyclic stability trends observed in DMSO.

The only inconsistency was in the trends for the distal N-protonated and N-methylated cationic balances **4** and **6**, as noted in the last section. In $CDCl_3$, the N-protonated balance **4** had a stronger interaction, whereas in DMSO-d_6, the N-methylated balance **6** had a stronger interaction. In CD_3CN, the two balances had very similar interaction energies. The greater solvent effects for these distal balances may be due to the greater interaction of solvents with the charged cationic surfaces in **4** and **6**. This may be due to the more solvent-exposed positive charge of the distal geometries. By comparison, the more shielded positive charge of the proximal balances (**5** and **7**) shows much smaller solvent effects and consistent *N*-methyl versus N-proton trends in each solvent. These differences could also be due to differences in solvation of the different counterions (I^- and MsO^-) for the N-methylated and N-protonated distal balances (**4** and **6**), respectively.

Table 3. Measured Relative Energies ($\Delta\Delta G$, kcal/mol)[a] of the N-Heterocyclic Balances 2-7 Relative to the Nonheterocyclic Balance 1

			$\Delta\Delta G^a$		
balance	π-stacking interaction	geometry	$CDCl_3$	CD_3CN	DMSO-d_6
1	Ph−Ph		0.00	0.00	0.00
2	Py−Ph	distal	−0.60	−0.54	−0.54
3		proximal	−0.19	−0.21	−0.37
4	PyH^+−Ph	distal	−0.89	−1.06	−0.77
5		proximal	−1.43	−1.66	−1.75
6	$PyMe^+$−Ph	distal	−0.40	−0.98	−1.08
7		proximal	≤−2.23	≤−1.89	≤−2.06

[a]The relative energy was quantified as $\Delta\Delta G = (\Delta G[\mathbf{x}] - \Delta G[\mathbf{1}])$; **x** = **2**−**7**; propagated uncertainty <±0.06 kcal/mol. The measured ΔG's for balances **1**−**7** in $CDCl_3$ and CD_3CN are included in Supporting Information Table S10.

Correlation with Benchmark-Quality Computational Calculations. Finally, the experimentally measured values in this study provided an opportunity to test the accuracy of current computational methods as well as the performance of our model system in accurately assessing N-heterocyclic π-stacking interactions. Benchmark quality calculations (CCSD-(T) or SCS−MP2 methods) from the literature for π-stacking interactions were used in the correlation analysis (Figure 11).[27,29,56] The geometries of the calculations were matched to

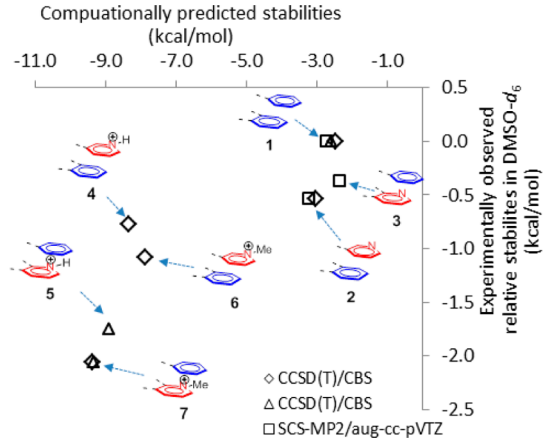

Figure 11. Correlation plot between the calculated energies from the benchmark quality computations in the literature and the experimentally observed relative energies ($\Delta\Delta G$'s) in DMSO-d_6 for the π-stacking interactions in balances **1**−**7**. The computational data were from ref 27 (open diamonds), ref 29 (open squares), and ref 56 (open triangles).

the geometries of the π-stacking interactions observed in the crystal structures of the balances, and the calculated interaction energies were matched to the experimentally measured relative energies ($\Delta\Delta G$) in DMSO-d_6 from Table 2.

The correlation plot showed a good general agreement between the computational and experimentally measured energies. For example, both methods provided similar stability trends: Ph−Ph < Py−Ph < (PyH^+−Ph and $PyMe^+$−Ph). There was also good agreement for the geometry-related stability trends (distal versus proximal) for both the neutral and cationic N-heterocyclic π-stacking interactions. For example, both methods found that the distal geometry was more stable for

dx.doi.org/10.1021/jo400370e | J. Org. Chem. 2013, 78, 5303−5313

the neutral Py−Ph stacking interaction, whereas the proximal geometry was more stable for the cationic PyH^+−Ph and $PyMe^+$−Ph stacking interactions.

Two minor deviations in the experimental and calculated trends were observed. The first deviation was that the neutral and cationic N-heterocyclic π-stacking interactions appeared to form separate trend lines on the correlation plot. This may be explained by the different environments (vacuum versus solvent) of the two methods. The solvent in the experimental studies more strongly screened the electrostatic interactions of the charged groups, which reduces their interaction strengths as compared with the in vacuo computational studies.

The second inconsistency was that the experimental study found that the proximal Py−Ph interaction in **3** was slightly stronger than the Ph−Ph stacking interaction in **1**. This trend is in opposition to the computational studies that predicted that positioning an electronegative nitrogen over an opposing aromatic π-surface in the proximal geometry should be a destabilizing interaction. We attribute this deviation to the mobility of the phenyl arm in solution, which allows the balance to also adopt geometries that avoid this destabilizing interaction. This minimizes the contribution of the destabilizing interaction to the closed/open ratio and leads to an overestimation of the strength of the proximal Py−Ph stacking interaction in balance **3**. It should be pointed out that the mobility of the arene arm will have less of an impact on balances that contain only attractive stabilizing interactions because the arm will preferentially seek out and adopt these more stable geometries.

Evaluation of the Design of the Molecular Balances. Overall, our *N*-arylimide bicyclic balance model system appeared to provide an effective platform to systematically and quantitatively study many aspects of the N-heterocyclic π-stacking interaction. However, as with all model systems, we had a number of concerns. In this section, we reanalyzed the data to check whether each concern was warranted.

The first concern was that the repulsive O−π interaction between the oxygen linker of the arm and the arene shelf might obscure or prevent accurate comparisons of the intramolecular π-stacking interactions of interest. However, this repulsive interaction was actually found to be an advantageous feature, which enabled more accurate measurement of the stronger N-heterocyclic π-stacking interaction. The maximum strength of the intramolecular interactions that can be measured by our balances is limited by the highest closed/open ratio that can be accurately measured. On the basis of a conservative detection limit of 5% of ^{1}H NMR spectra,[57,58] the highest closed/open ratio that can be measured is 19:1. If the closed/open ratio in the absence of the interaction was 1:1, this would correspond to a maximum measurable interaction energy of only −1.74 kcal/mol. This low limit is particularly important for this study because the cationic N-heterocyclic π-stacking interactions were all stronger than −2.0 kcal/mol. However, the repulsive interactions of the oxygen linkers in our balances act like a "spring", which shifts the resting state of the balance toward the open conformer to give a closed/open ratio of ∼1:7 in DMSO-d_6.[40] This spring effect allows for a larger change in closed/open ratio from 1:7 to 19:1, which corresponds to a maximum measurable interaction of up to −2.88 kcal/mol.

A second design concern was whether we could compare balances with N-heterocycles in the arm against those with N-heterocycles in the shelf. These two surfaces are not identical and possess different degrees of π-conjugation. However, analysis of the ΔG's for balances **1**−**7** suggested that this concern was unwarranted or was very minor because the expected stability trends (Ph−Ph < Py−Ph < (PyH^+−Ph and $PyMe^+$−Ph)) were clearly observed. More importantly, the expected and more subtle geometry-related stability trends (proximal versus distal) were accurately reproduced by the molecular balances. These geometry-related trends relied on directly comparing balances with N-heterocycles in the arm and shelf.

A third design concern was whether the mobility of the arm arene in the closed conformer balances would compromise their ability to distinguish the distal and proximal geometries of the N-heterocyclic π-stacking interactions. Generally, the expected distal versus proximal stability trends were observed. However, the ability of the arene arm to slide back and forth across the arene shelf could lead to underestimations of the difference in energy of proximal and distal geometries when destabilizing repulsive interactions are involved. To address this problem, we are currently utilizing advanced NMR methods, such as through-space coupling and nuclear Overhauser effects to investigate the mobility of the arene arm and measuring the population of various subconformations to refine the energy calculations.

The last design concern was the asymmetry of the cationic aromatic shelves in balances **5** and **7**. Ideally, both heterocyclic nitrogens would be charged so that the arm arene could form the same π-stacking interactions with either outer ring of the arene shelf, but this was not synthetically feasible. Clearly, these singly charged balances are still able to form the expected cation-π interactions because these balances had significantly stronger π-stacking interactions than their neutral counterparts. This highlights one advantage of arm mobility in the study of attractive interactions: the arms will preferentially form the more stabilizing π-stacking interaction with the cationic versus neutral outer ring. However, we cannot eliminate the possibility that the ability of these balances to also form the neutral π-stacking interaction may lead to an underestimation of the energies of the cationic π-stacking interactions in balances **5** and **7**. Again, advanced NMR techniques will be applied in future studies to quantify the contribution of these less stable geometries.

■ CONCLUSIONS

A new series of molecular balance model systems (**2**−**7**) were designed and used to perform a comprehensive study of the influences of position, charge, and substitution of the nitrogen atom on N-heterocyclic π-stacking interactions in the solid state and in solution. The formation and geometry of the intramolecular N-heterocyclic π-stacking interactions in the closed conformation models were verified via X-ray crystallographic analysis in the solid state. The relative stabilities of these N-heterocyclic π-stacking interactions in solution were systematically studied by comparing the closed/open ratios of the corresponding molecular balances that were measured via integration of the ^{1}H NMR spectra. The stability trend Ph−Ph < Py−Ph < (PyH^+−Ph and $PyMe^+$−Ph) was quantitatively measured for the first time within a single model system. The position of the heterocyclic nitrogen was found to influence the strengths of both the neutral and cationic N-heterocyclic π-stacking interactions, leading to opposite stability trends. For the neutral Py−Ph stacking interaction, the distal geometry was found to be slightly more favorable. For the cationic PyH^+−Ph and $PyMe^+$−Ph stacking interactions, the proximal geometry

dx.doi.org/10.1021/jo400370e | J. Org. Chem. 2013, 78, 5303−5313

was found to be significantly more favorable. The influence of N-methylation and N-protonation was also compared. For the proximal complex, the PyMe$^+$−Ph interaction was found to be significantly stronger than the PyH$^+$−Ph stacking interaction. This was attributed to the formation of additional CH−π interaction between the *N*-methyl proton and the opposing phenyl ring. The measured trends were consistently observed in three common organic solvents (chloroform, acetonitrile, and DMSO), confirming the generality of these trends. The experimentally measured stabilities for the N-heterocyclic π-stacking interactions in balances **1**−**7** were found to generally agree with the corresponding benchmark quality computational values in the literature. Discrepancies were mainly attributed to the presence of solvent in the experimental studies and the difficulties in experimentally measuring the interaction strength of unfavorable geometries.

The quantitatively measured stability trends for the N-heterocyclic π-stacking interactions provide guidance in the design and optimization of applications that rely on these molecular recognition processes. For example, insertion of N-heterocycles will strengthen attractive aromatic π-stacking interactions, but only if the nitrogen atoms are appropriately positioned away from the π-face of the opposing aromatic surface. The insertion of positively charged N-heterocycles also provides a simple means to significantly strengthen the π-stacking interaction, but these charged heteroarenes also impose an even stronger directional preference. Finally, to study the stability trends for the noncovalent interactions of aromatic surfaces in more biologically relevant aqueous environments, we have developed a water-soluble version of these molecular balances and will be reporting these results in future studies.

EXPERIMENTAL SECTION

General Experimental. All chemicals were purchased from commercial suppliers and used as received unless otherwise noted. All reactions were carried out under a dry N_2 atmosphere in oven−dried glassware. Dry organic solvents were obtained by passing the degassed solvents through activated alumina columns. Flash chromatography was carried out using either silica gel (60 Å, 200−400 mesh) or aluminum oxide (60 Å, 20−200 mesh) as noted. Thin layer chromatography for monitoring the reaction progress was performed using either precoated 0.25 mm silica gel 60 F254 plates or precoated 0.25 mm aluminum oxide 60 F254 plates. NMR spectra were recorded on 300 MHz, 400 MHz spectrometers. Chemical shifts are reported in parts per million (δ) and were referenced to TMS. HRMS was recorded with a magnetic sector spectrometer using EI sources and the Q-TOF 1 spectrometer using ESI sources.

Balances **1** and **1′**, anhydride **11**, *N*-(2-phenyloxyl)phenyl maleimide (**17**), and *N*-(2,6-diphenoxylphenyl) maleimide were prepared utilizing our previously described routes for the analogous parent compounds.[40] Diene **13**[44] and *ortho*-pyridin-3-ylaniline (**10**)[42] were obtained using literature procedures.

*(9R,9aS,12aR,13S)-9,13-Dimethyl-11-(2-phenoxyphenyl)-12a,13-dihydro-9H-9,13-methanophenanthro[9,10-f]-isoindole-10,12,14(9aH,11H)-trione (**1″**).* Diene **16** (0.20 g, 0.77 mmol) and *N*-(2-phenyloxylphenyl) maleimide (**17**) (0.24 g, 0.92 mmol) were dissolved in dry toluene (10 mL). The mixture was stirred and heated at reflux under N_2 for 24 h. The solvent was removed under vacuum to give a light yellow solid. Recrystallization from ethanol gave diene **1″** as a white crystalline solid (0.36 g, 87%). mp 310 °C dec. ^{1}H NMR (400 MHz, $CDCl_3$) δ 8.79 (dd, J = 8.3 Hz, J = 1.2 Hz, 2H major), 8.38 (dd, J = 8.2 Hz, J = 1.3 Hz, 2H major), 8.26 (dd, J = 8.3 Hz, J = 1.0 Hz, 2H minor), 8.14 (dd, J = 8.4 Hz, J = 1.0 Hz, 2H minor), 7.61−7.72 (m, 4H major), 6.81−7.49 (m, 5H major, 12H minor), 6.65 (dd, J = 8.3 Hz, J = 1.2 Hz, 1H major), 6.44 (td, J = 7.7 Hz, J = 1.3 Hz, 1H major), 5.96 (dd, J = 8.4 Hz, J = 1.2 Hz, 1H minor), 5.73−5.78 (m, 1H major), 4.68 (dd, J = 7.9 Hz, J = 1.6 Hz, 1H major), 3.60 (s, 2H minor), 3.42 (s, 2H major), 2.31 (s, 3H major), 2.28 (s, 3H minor). ^{13}C NMR (100 MHz, $CDCl_3$): 201.1, 199.6, 174.2, 173.7, 156.2, 153.0, 133.3, 133.1, 130.9, 130.8, 130.4, 129.9, 129.3, 128.9, 128.2, 127.5, 127.4, 127.3, 126.7, 126.5, 125.3, 125.0, 124.2, 123.5, 123.4, 123.3, 121.8, 121.7, 121.6, 119.5, 118.8, 116.1, 77.5, 77.2, 77.2, 76.8, 55.2, 55.1, 48.4, 47.9, 14.8. HRMS (EI) m/z calcd for $C_{35}H_{25}NO_4$ (M^+): 523.1784; found: 523.1778.

*(9R,9aS,12aR,13S)-9,13-Diphenyl-11-(2-(pyridin-3-yloxy)-phenyl)-12a,13-dihydro-9H-9,13-methanophenanthro[9,10-f]isoindole-10,12,14(9aH,11H)-trione (**2**).* To a solution of anhydride **11** (0.29 g, 0.60 mmol) in acetic acid (25 mL), *ortho*-pyridine-3-ylaniline (**10**) (0.15 g, 0.81 mmol) was added. The mixture was stirred and heated at reflux under N_2 for 24 h. The solvent was removed under vacuum to give a brown solid. The solid was suspended in Na_2CO_3 aqueous solution (50 mL) and then extracted with CH_2Cl_2 (3 × 30 mL). The organic layer was collected, washed with brine (30 mL), and dried over $MgSO_4$. The solvent was removed under vacuum to give a brown solid. Flash chromatography (aluminum oxide, MeOH/CH_2Cl_2 = 1/100) provided **2** as a pale white solid (0.29 g, 81%). mp 280 °C dec. ^{1}H NMR (400 MHz, $CDCl_3$) δ 8.73 (d, J = 8.5 Hz, 2H minor), 8.45−8.35 (m, 2H minor, 2H major), 8.33−8.26 (m, 1H major, 2H minor), 8.16 (d, J = 8.5 Hz, 2H major), 6.86−7.75 (m, 19H major and 16H minor), 6.65 (dd, J = 8.3 Hz, J = 1.1 Hz, 1H minor), 6.47 (td, J = 7.9 Hz, J = 1.1 Hz, 1H minor), 6.18 (ddd, J = 8.3 Hz, J = 2.6 Hz, J = 1.4 Hz, 1H major), 5.93 (dd, J = 8.3 Hz, J = 1.1 Hz, 1H major), 4.68 (s, 2H major), 4.64 (dd, J = 7.9 Hz, J = 1.6 Hz, 1H minor), 4.58 (s, 2H minor). ^{13}C NMR (100 MHz, $CDCl_3$): 197.0, 195.7, 173.5, 173.0, 154.4, 152.5, 150.5, 145.7, 145.5, 143.8, 142.4, 133.9, 133.7, 133.7, 133.5, 131.3, 131.2, 131.1, 130.9, 130.7, 129.5, 129.4, 129.3, 129.2, 129.1, 128.9, 128.8, 128.6, 128.5, 128.4, 127.4, 127.0, 126.8, 126.7, 126.4, 126.3, 126.2, 126.0, 125.9, 124.4, 124.1, 123.9, 123.1, 122.9, 122.6, 122.2, 120.8, 118.4, 116.0, 77.5, 77.2, 77.1, 76.8, 63.7, 63.6, 45.6, 45.2. HRMS (EI) m/z calcd for $C_{44}H_{28}N_2O_4$ (M^+): 648.2049; found: 648.2059.

*(9R,9aS,12aR,13S)-9,13-Dimethyl-11-(2-phenoxyphenyl)-12a,13-dihydro-9H-9,13-methanoisoindolo[5,6-f][1,10]-phenanthroline-10,12,14(9aH,11H)-trione (**3**).* Diene **13** (0.20 g, 0.77 mmol) and *N*-(2-phenyloxylphenyl) maleimide (**17**) (0.24 g, 0.92 mmol) were dissolved in CH_2Cl_2 (15 mL) and sealed in a medium pressure tube after flushing with N_2. The pressure tube was heated to 90 °C with stirring for 24 h. After cooling, the solvent was removed under vacuum. The solid residue was washed with cold acetonitrile and acetone to give **3** as an off-white solid (0.18 g, 45%). mp 280 °C dec. ^{1}H NMR (400 MHz, $CDCl_3$) δ 9.18 (d, J = 4.2 Hz, 2H major), 8.82 (d, J = 4.2 Hz, 2H minor), 8.67 (d, J = 8.4 Hz, 2H major), 8.48 (d, J = 8.4 Hz, 2H minor), 7.63 (dd, J = 8.4 Hz, J = 4.3 Hz, 2H major), 7.29 (dd, J = 8.4 Hz, J = 4.3 Hz, 2H minor), 6.75−7.25 (m, 5H major and 8H minor), 6.61 (d, J = 8.3 Hz, 1H major), 6.42 (t, J = 7.7 Hz, 1H major), 5.90−5.99 (m, 1H major, 1H minor), 4.68 (dd, J = 7.9 Hz, J = 1.1 Hz, 1H major), 3.56 (s, 2H

dx.doi.org/10.1021/jo400370e | J. Org. Chem. 2013, 78, 5303−5313

minor), 3.41 (s, 2H major), 2.25 (s, 3H major), 2.21 (s, 3H minor). ^{13}C NMR (100 MHz, $CDCl_3$): 199.9, 198.6, 173.7, 173.4, 155.9, 154.8, 153.7, 152.6, 150.8, 149.9, 146.4, 146.1, 133.3, 133.1, 132.6, 132.0, 130.7, 130.5, 129.9, 129.6, 128.4, 127.8, 124.8, 124.6, 124.4, 124.2, 123.5, 122.8, 121.7, 121.5, 121.2, 119.9, 119.4, 118.7, 116.6, 77.5, 77.2, 77.1, 76.8, 55.4, 55.3, 47.9, 47.5, 14.4, 14.2. HRMS (EI) m/z calcd for $C_{33}H_{23}N_3O_4$ (M^+): 525.1689; found: 525.1679.

*(9R,9aS,12aR,13S)-11-(2,6-Diphenoxyphenyl)-9,13-dimethyl-12a,13-dihydro-9H-9,13-methanoisoindolo[5,6-f][1,10]phenanthroline-10,12,14(9aH,11H)-trione (**3′**).* Diene **13** (0.20 g, 0.75 mmol) and *N*-(2,6-diphenoxylphenyl) maleimide (**18**) (0.32 g, 0.75 mmol) were reacted using the same procedure as described for balance **3**. The product **3′** was obtained as a pale white solid (0.28 g, 60%). mp 280 °C dec. ^{1}H NMR (400 MHz, $CDCl_3$) δ 8.98−9.01 (m, 2H), 8.69 (dd, J = 8.4 Hz, J = 1.3 Hz, 2H), 6.93−7.55 (m, 11H), 6.45 (d, J = 8.2 Hz, 1H), 6.12 (d, J = 7.7 Hz, 2H), 5.85 (d, J = 8.5 Hz, 1H), 3.63 (s, 2H), 2.37 (s, 6H). ^{13}C NMR (100 MHz, $CDCl_3$): 198.8, 173.2, 156.3, 155.8, 153.7, 149.7, 146.3, 133.1, 131.9, 130.3, 129.9, 129.5, 124.8, 124.4, 124.3, 122.6, 121.2, 119.5, 111.4, 111.0, 110.6, 77.4, 77.1, 76.8, 55.2, 47.7, 14.2. HRMS (EI) m/z calcd for $C_{39}H_{27}N_3O_5$ (M^+): 617.1951; found: 617.1939.

*1-Methyl-3-(2-((9R,9aR,12aS,13S)-10,12,14-trioxo-9,13-diphenyl-9a,10,12a,13-tetrahydro-9H-9,13-methanophenanthro[9,10-f]isoindol-11(12H)-yl)phenoxy)-pyridin-1-ium iodide (**6**).* To a solution of balance **2** (0.20 g, 0.31 mmol) in acetone (40 mL), methyl iodide (1.0 mL, 16.1 mmol) was added. The reaction mixture was stirred at 45 °C for 12 h in the dark under N_2. After cooling to room temperature, a yellow precipitate was collected by filtration and washed with cold acetone to quantitatively give **6** as a yellow solid (0.25 g, 100%). mp 240 °C. ^{1}H NMR (400 MHz, DMSO-d_6) δ 8.99−9.02 (m, 1H minor), 8.94 (d, J = 8.5 Hz, 2H minor), 8.79−8.83 (m, 1H minor), 8.73 (d, J = 6.0 Hz, 1H major), 8.51 (d, J = 8.5 Hz, 2H major), 8.31 (d, J = 7.8 Hz, 2H major), 8.20 (d, J = 7.8 Hz, 2H minor), 8.05−8.10 (m, 1H minor), 7.97−8.02 (m, 1H minor), 6.92−7.85 (m, 20H major, 17H minor), 6.63 (td, J = 7.9 Hz, J = 1.1 Hz, 1H minor), 6.31−6.36 (m, 1H major), 5.01 (s, 2H minor), 4.99 (s, 2H major), 4.44 (dd, J = 7.9 Hz, J = 1.6 Hz, 1H minor), 4.34 (s, 3H minor), 4.31 (s, 3H major). ^{13}C NMR (100 MHz, DMSO-d_6): 195.6, 174.0, 152.9, 152.4, 142.2, 138.8, 137.1, 133.98, 133.6, 131.0, 130.5, 129.1, 129.1, 128.3, 128.2, 126.5, 126.0, 125.8, 125.3, 124.4, 123.2, 121.8, 63.1, 62.9, 47.9, 45.3, 40.1, 39.9, 39.7, 39.5, 39.5, 39.3, 39.1, 38.9, HRMS (ESI) m/z calcd for cation $[C_{45}H_{31}N_2O_4]^+$ (M^+): 663.2284; found: 663.2277.

*(9S,9aR,12aS,13R)-4,9,13-Trimethyl-10,12,14-trioxo-11-(2-phenoxyphenyl)-9a,10,11,12,12a,13-hexahydro-9H-9,13-methanoisoindolo[5,6-f][1,10]phenanthrolin-4-ium iodide. (**7**).* To a solution of balance **3** (80 mg, 0.15 mmol) in acetone (20 mL), methyl iodide (0.47 mL, 7.55 mmol) was added. The reaction mixture was heated at reflux for 12 h in the dark under N_2. After cooling to room temperature, a yellow precipitate was collected by filtration and washed with cold acetone to quantitatively give **7** as a yellow powder (102 mg, 100%). mp 280 °C dec. The racemic form **7** was used without resolution. ^{1}H NMR (400 MHz, DMSO-d_6) δ 9.34 (d, J = 8.5 Hz, 1H), 9.12−9.19 (m, 2H), 8.87 (d, J = 8.6 Hz, 1H), 8.10 (dd, J = 8.4 Hz, J = 5.9 Hz, 1H), 7.98 (dd, J = 8.4 Hz, J = 4.2 Hz, 1H), 6.89−7.31 (m, 6H), 5.90 (d, J = 8.4 Hz, 1H), 5.82 (d, J = 7.5 Hz, 2H), 4.86 (s, 3H), 4.04 (s, 2H), 2.20 (s, 3H), 2.19 (s, 3H). ^{13}C NMR (100 MHz, $CDCl_3$): 198.3, 174.3, 174.1, 154.1, 153.5, 150.4, 149.1, 141.8, 140.3, 137.9, 137.4, 133.4, 132.9, 130.6, 129.9, 129.5, 127.7, 126.9, 125.3, 125.2, 124.5, 122.3, 120.6, 120.5, 115.8, 54.9, 54.9, 54.8, 47.5, 47.4, 40.2, 39.9, 39.7, 39.52, 39.5, 39.3, 39.1, 38.9, 13.9, 13.5. HRMS (ESI) m/z calcd for cation $[C_{34}H_{26}N_3O_4]^+$ (M^+): 540.1923; found: 540.1918.

■ ASSOCIATED CONTENT

Ⓢ Supporting Information

Additional figures and tables. Copies of ^{1}H and ^{13}C NMR spectra for all the newly synthesized molecular balances. X-crystal data (CIF) of **1″**, **2**, **3**, **3′**, **4**, **6**, and **7**. Characterization of the O−π repulsion in crystal structures. Quantification of the open and closed conformers in solution. The error analysis and maximum closed/open ratio. This material is available free of charge via the Internet at http://pubs.acs.org.

■ AUTHOR INFORMATION

Corresponding Author

*Tel: (803)7776523. Fax: (803)7779521. E-mail: shimizu@mail.chem.sc.edu.

Notes

The authors declare no competing financial interest.

■ ACKNOWLEDGMENTS

This work was supported by the National Science Foundation Grants Nos. CHE-0911616 and CHE-1048629.

■ REFERENCES

(1) Meyer, E. A.; Castellano, R. K.; Diederich, F. *Angew. Chem., Int. Ed.* **2003**, *42*, 1210.
(2) Salonen, L. M.; Ellermann, M.; Diederich, F. *Angew. Chem., Int. Ed.* **2011**, *50*, 4808.
(3) Jaffe, R. L.; Smith, G. D. *J. Chem. Phys.* **1996**, *105*, 2780.
(4) Hobza, P.; Selzle, H. L.; Schlag, E. W. *J. Phys. Chem.* **1996**, *100*, 18790.
(5) Tsuzuki, S.; Honda, K.; Uchimaru, T.; Mikami, M.; Tanabe, K. *J. Am. Chem. Soc.* **2002**, *124*, 104.
(6) Sinnokrot, M. O.; Valeev, E. F.; Sherrill, C. D. *J. Am. Chem. Soc.* **2002**, *124*, 10887.
(7) Sinnokrot, M. O.; Sherrill, C. D. *J. Phys. Chem. A* **2004**, *108*, 10200.
(8) Sinnokrot, M. O.; Sherrill, C. D. *J. Am. Chem. Soc.* **2004**, *126*, 7690.
(9) Tsuzuki, S.; Uchimaru, T.; Mikami, M. *J. Phys. Chem. A* **2006**, *110*, 2027.
(10) Ringer, A. L.; Sherrill, C. D. *J. Am. Chem. Soc.* **2009**, *131*, 4574.
(11) Cozzi, F.; Cinquini, M.; Annunziata, R.; Dwyer, T.; Siegel, J. S. *J. Am. Chem. Soc.* **1992**, *114*, 5729.
(12) Cozzi, F.; Ponzini, F.; Annunziata, R.; Cinquini, M.; Siegel, J. S. *Angew. Chem., Int. Ed. Engl.* **1995**, *34*, 1019.
(13) Rashkin, M. J.; Waters, M. L. *J. Am. Chem. Soc.* **2002**, *124*, 1860.
(14) Gung, B. W.; Patel, M.; Xue, X. W. *J. Org. Chem.* **2005**, *70*, 10532.
(15) Gung, B. W.; Xue, X. W.; Reich, H. J. *J. Org. Chem.* **2005**, *70*, 3641.
(16) Cockroft, S. L.; Hunter, C. A.; Lawson, K. R.; Perkins, J.; Urch, C. J. *J. Am. Chem. Soc.* **2005**, *127*, 8594.
(17) Gung, B. W.; Amicangelo, J. C. *J. Org. Chem.* **2006**, *71*, 9261.
(18) Cockroft, S. L.; Perkins, J.; Zonta, C.; Adams, H.; Spey, S. E.; Low, C. M. R.; Vinter, J. G.; Lawson, K. R.; Urch, C. J.; Hunter, C. A. *Org. Biomol. Chem.* **2007**, *5*, 1062.
(19) Gung, B. W.; Emenike, B. U.; Alverez, C. N.; Rakovan, J.; Kirschbaum, K.; Jain, N. *Tetrahedron Lett.* **2010**, *51*, 1648.
(20) Yamada, S. *Org. Biomol. Chem.* **2007**, *5*, 2903.

(21) Yamada, S.; Fossey, J. S. *Org. Biomol. Chem.* **2011**, *9*, 7275.
(22) Saenger, W. *Principles of nucleic acid structure*; Springer-Verlag: New York, 1984.
(23) Li, X. M.; Liu, P.; Houk, K. N.; Birman, V. B. *J. Am. Chem. Soc.* **2008**, *130*, 13836.
(24) Hunter, C. A. *J. Mol. Biol.* **1993**, *230*, 1025.
(25) Geerlings, P.; Mignon, P.; Loverix, S.; De Proft, F. *J. Phys. Chem. A* **2004**, *108*, 6038.
(26) Mishra, B. K.; Sathyamurthy, N. *J. Phys. Chem. A* **2005**, *109*, 6.
(27) Tsuzuki, S.; Mikami, M.; Yamada, S. *J. Am. Chem. Soc.* **2007**, *129*, 8656.
(28) Wang, W. Z.; Hobza, P. *ChemPhysChem* **2008**, *9*, 1003.
(29) Hohenstein, E. G.; Sherrill, C. D. *J. Phys. Chem. A* **2009**, *113*, 878.
(30) Smith, Q. A.; Gordon, M. S.; Slipchenko, L. V. *J. Phys. Chem. A* **2011**, *115*, 4598.
(31) Mati, I. K.; Cockroft, S. L. *Chem. Soc. Rev.* **2010**, *39*, 4195.
(32) McKay, S. L.; Haptonstall, B.; Gellman, S. H. *J. Am. Chem. Soc.* **2001**, *123*, 1244.
(33) Gung, B. W.; Wekesa, F.; Barnes, C. L. *J. Org. Chem.* **2008**, *73*, 1803.
(34) Kearney, P. C.; Mizoue, L. S.; Kumpf, R. A.; Forman, J. E.; McCurdy, A.; Dougherty, D. A. *J. Am. Chem. Soc.* **1993**, *115*, 9907.
(35) Rashkin, M. J.; Hughes, R. M.; Calloway, N. T.; Waters, M. L. *J. Am. Chem. Soc.* **2004**, *126*, 13320.
(36) Grimme, S. *Angew. Chem., Int. Ed.* **2008**, *47*, 3430.
(37) Wheeler, S. E.; Houk, K. N. *J. Am. Chem. Soc.* **2008**, *130*, 10854.
(38) Wheeler, S. E. *J. Am. Chem. Soc.* **2011**, *133*, 10262.
(39) Martinez, C. R.; Iverson, B. L. *Chem. Sci.* **2012**, *3*, 2191.
(40) Carroll, W. R.; Pellechia, P.; Shimizu, K. D. *Org. Lett.* **2008**, *10*, 3547.
(41) Carroll, W. R.; Zhao, C.; Smith, M. D.; Pellechia, P. J.; Shimizu, K. D. *Org. Lett.* **2011**, *13*, 4320.
(42) Huang, D. H.; Poon, S. F.; Chapman, D. F.; Chung, J.; Cramer, M.; Reger, T. S.; Roppe, J. R.; Tehrani, L.; Cosford, N. D. P.; Smith, N. D. *Bioorg. Med. Chem. Lett.* **2004**, *14*, 5473.
(43) You, F. X.; Twieg, R. J. *Tetrahedron Lett.* **1999**, *40*, 8759.
(44) Warrener, R. N.; Schultz, A. C.; Houghton, M. A.; Butler, D. N. *Tetrahedron* **1997**, *53*, 3991.
(45) Fuchs, B.; Pasternak, M. *Tetrahedron* **1981**, *37*, 2501.
(46) Janiak, C. *J. Chem. Soc., Dalton Trans.* **2000**, 3885.
(47) Chelli, R.; Gervasio, F. L.; Procacci, P.; Schettino, V. *J. Am. Chem. Soc.* **2002**, *124*, 6133.
(48) McCurdy, A.; Jimenez, L.; Stauffer, D. A.; Dougherty, D. A. *J. Am. Chem. Soc.* **1992**, *114*, 10314.
(49) Yamada, S. J.; Uematsu, N.; Yamashita, K. *J. Am. Chem. Soc.* **2007**, *129*, 12100.
(50) Yamada, S.; Morita, C. *J. Am. Chem. Soc.* **2002**, *124*, 8184.
(51) Barin, G.; Coskun, A.; Fouda, M. M. G.; Stoddart, J. F. *ChemPlusChem* **2012**, *77*, 159.
(52) Nijamudheen, A.; Jose, D.; Shine, A.; Datta, A. *J. Phys. Chem. Lett.* **2012**, *3*, 1493.
(53) Hunter, C. A.; Sanders, J. K. M. *J. Am. Chem. Soc.* **1990**, *112*, 5525.
(54) Nishio, M.; Umezawa, Y.; Honda, K.; Tsuboyama, S.; Suezawa, H. *CrystEngComm* **2009**, *11*, 1757.
(55) Hughes, R. M.; Waters, M. L. *J. Am. Chem. Soc.* **2005**, *127*, 6518.
(56) Singh, N. J.; Min, S. K.; Kim, D. Y.; Kim, K. S. *J. Chem. Theory Comput.* **2009**, *5*, 515.
(57) Rizzo, V.; Pinciroli, V. *J. Pharm. Biomed. Anal.* **2005**, *38*, 851.
(58) Malz, F.; Jancke, H. *J. Pharm. Biomed. Anal.* **2005**, *38*, 813.